Swelling of a hemi-ellipsoidal ionic hydrogel for determination of material properties of deposited thin polymer films: an inverse finite element approach

Victorien Prot[1], Hrafn Mar Sveinsson[2], Kamila Gawel[2], Ming Gao[2], Bjørn Skallerud[1] and Bjørn Torger Stokke[2*]

[1]Biomechanics Division, Department of Structural Engineering, The Norwegian University of Science and Technology, NTNU, NO-7491 Trondheim, Norway
[2]Biophysics and Medical Technology, Department of Physics, The Norwegian University of Science and Technology, NTNU, NO-7491 Trondheim, Norway
[*]Corresponding author

Abstract

Selective deposition of polymers at the surface of an ionic hydrogel is conventionally used to tailor properties of the composite material for application within for instance drug release and cell encapsulation. Here we describe a method for determination of the mechanical properties of a thin polymer film deposited on an ionic hydrogel core. The ionic strength-dependent hydrogel swelling is affected by the crosslink density and thickness of the deposited polymer layer. A hemi-ellipsoidal geometry of the hydrogel, corresponding to that employed in proof-of-concept experiments, is used to enforce biaxial deformation of the deposited layer when the ionic hydrogel core is equilibrated at various ionic strengths. The ionic strength dependent equilibrium swelling ratio of the hydrogel with deposited polymer film is modeled using a finite element approach. The free energy of the hydrogel core includes contributions accounting for the polymer mixing, the elastic deformation of the network and the Donnan equilibrium. The latter type of contribution is not included in the neutral thin layer in the present study. Adding the polymer multilayer/shell at the surface reveals that the ionic strength-dependent swelling constraint is more pronounced the thicker and stiffer the film is. Combining thickness measurements of the polymer film with high resolution interferometric determination of reduction in swelling capacity of ionic hydrogels, an equivalent elastic property of the polymer layer is obtained using inverse finite element analysis. In the proof-of-concept experiments, analysis of data obtained for chitosan-alginate multilayers composed of four and eight polymer bilayers deposited on anionic acrylamide-based hydrogel core suggest that these bilayers show an elastic stiffness one order of magnitude larger than the one of the hydrogel core.

1 Introduction

Hydrogels made from either synthetic or natural polymers are three-dimensional networks stabilized by covalent or physical bonds, and contain a large fraction of water. The physico-chemical properties of these soft materials can be changed by subsequent deposition of a polymer layer at the hydrogel surface.[1,2] Layered polymer deposition is explored as an aid for surface functionalization to increase biocompatibility of mechanically tunable hydrogel materials[3], to control permeability and stability of matrices used for immobilization of living cells[4] and in drug delivery[5]. Similar layered structuring is also reported for surfactant deposition on highly charged hydrogels, yielding a balloon type structure with the surfactant deposition at the surface making up a shell. The swelling of such composite materials exposed to various ionic strengths displays a balloon-like character that may lead to bursting. Although the role of the layered polymer or surfactant deposition in these cases differ, the properties of the finally prepared composite soft material are affected by the mechanical properties of the outer shell.

Surface functionalization of polyacrylamide hydrogels with collagen type I was quite recently shown to tune elasticity and biocompatibility of hydrogel materials. Possible impact of mechanical cues on differentiation of human mesenchymal stem cells was discussed[3]. Mechanical characterization of the composite material using nanoindentation indicates an increase of the effective Young's modulus when compared to the non-functionalized hydrogel starting material.

Following the initial report on a bioartificial pancreas in 1980[6], hydrogel capsules of alginate subjected to a subsequent polycation coating have been widely studied systems for microencapsulation of insulin producing cells. Immobilization of living cells employing ionotropic alginate gelation is explored as a necessary step to provide immunoisolated cells for prospective transplantation. In addition to requirements on e.g. biocompatibility and permeability, successful application of immunoisolated cells using gel bead embedding also require mechanical stability over the duration of the implantation[7–9]. The hydrogel coating by polycation is reported to affect the mechanical stability[7] and the swelling capacity of multilayer coated alginate beads[8]. Although these findings clearly indicate that polycation deposition at the surface affects the behavior of the resulting composite material through its mechanical properties, the direct determination of the layer mechanical properties was not explored. A step toward determining a relationship between thickness of deposited shell and mechanical properties of resulting composite was done by Yamanlar et al.[4]. Deposition of poly(L-lysine)/hyaluronic acid multilayers on a hyaluronic acid hydrogel surface was shown to increase hydrophobicity, reduce hydrogel equilibrium swelling ratio and increase compressive moduli of the material. The surface modification resulted in improved cell attachment and spreading of NIH-3T3 fibroblasts.

In all the above examples, the mechanical properties of the deposited film remain insufficiently characterized. Mechanical testing of polyelectrolyte multilayers and reinforced polymer gels are challenging in the sense that they constitute soft materials of very small dimensions, where nanomechanical characterization appears to be the most viable route. Surface wrinkling of films deposited on softer matrices is established as an experimental method for determination of mechanical properties of the films[9,10]. This method, applicable for substrates with Young's modulus larger than about 100 kPa, also requires a modulus mismatch between the layer and the substrate of about one order of magnitude. Thus, the method does not cover the range typically encountered for e.g. alginate hydrogels used for immobilization of cells[11] or model substrates for assessment of mechanical cues on cell differentiation[3].

In the following, we suggest a method to find the elastic property of such thin polymer layer deposits on

hydrogels by determination of the ionic strength induced swelling of a hemi-ellipsoidal hydrogel substrate before and after the thin film deposition.
Selecting a range of mechanical stiffnesses and layer thicknesses in the model for the film combined with the appropriate material parameters for the hydrogel substrate, a two-dimensional calibration plot of reduced swelling capacities was constructed using a finite element approach with a hyperelastic material model presented by Marcombe et al.[12]. Thus, experimental determination of the reduction of swelling due to the polymer coating and coating thickness allow determination of the deposited film's mechanical properties. This strategy is realized using a hemi-ellipsoidal geometry that is both coinciding with the experimental proof of concept realization[11], and that ensures nearly uniform deformation of the polymer coating.
This approach is realized by interferometric swelling measurements of hemi-ellipsoidal hydrogels as a function of ionic strengths before and after the deposition of the polymer layer coating, see Figure 1. The high precision measurements of the optical length of the hydrogel (2 nm) for the swelling of a hemi-ellipsoidal hydrogel with radius of about 50 μm yields a relative precision of about 0.001% in swelling. The optical fiber interferometry facilitates determination of the mechanical parameter of the layer with higher precision than hydrogel swelling data obtained by less precise techniques such as optical imaging using a light microscope, or gravimetric analysis.

The present work is organized as follows. In Section 2 we present the experimental method for determination of the reduction of swelling with and without the polymer coating and the constitutive material models used for the hydrogel and the polymer film. Then the finite element model used in this work and the numerical method employed to determine the material properties of the hydrogel and the deposited thin polymer film are described. In Section 3 the validation of our modeling approach is presented together with a two-dimensional calibration plot of reduced swelling capacities. Then constraining effects due the optical fiber and the deposited layer are exposed. Finally we give some concluding remarks.

2 Materials and Methods

2.1 Materials

Materials used for the synthesis of the hydrogel, for fluorescent labeling of chitosan and the polymer materials used for multilayer deposition were as follow: acrylamide (AAM, prop-2-enamide, 99%, Sigma), bisacrylamide (BIS, N,N-methylene-bis-acrylamide, 99%+, Acros organics), anionic monomer (AMPSA, 2-acrylamido-2-methylpropane sulfonic acid, 99%, Aldrich), photo initiator (hydroxy-cyclohexylphenylketone, 99%, Aldrich), squalane oil (2,6,10,15,19,23-hexamethyltetracosane, 99%, Aldrich), NaCl (sodium chloride, Sigma Aldrich, 99%)), CH_3COOH (acetic acid, pro analysis, Merck), NaOH (sodium hydroxide, pro analysis, Merck), fluorescent probe (Alexa Fluor 488 carboxylic acid succinimidyl ester, Invitrogen), dimethyl sulfoxide (DMSO, absolute, over molecular sieve ($H_2O \leq 0.01\%$), $\geq 99.5\%$ (GC), Sigma-Aldrich), chitosan (CHIT, degree of acetylation F_A=0.1, viscosity average Mv$\sim$300 kDa (kindly provided by prof Kjell Morten Vårum, Dept. of Biotechnology, NTNU, Trondheim) estimated based on reported parameters of Mark-Houwink-Kuhn-Sakurada relation[13], alginate from *Laminaria hyperborea* stem (ALG, viscosity average Mv$\sim$100 kDa, kindly provided by Dept. of Biotechnology, NTNU, Trondheim). All the solutions were prepared based on deionized water with resistivity 18 MΩ cm (Milli-Q, Millipore).

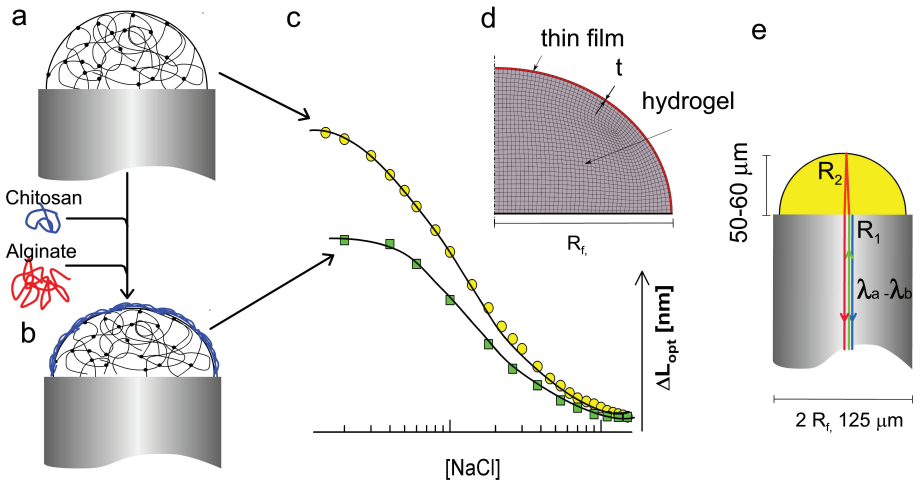

Fig. 1: Schematic illustration of the strategy implemented to determine mechanical properties of thin polymer films, e.g. multilayers, by comparison of ionic strength dependent swelling (c) of ionic hydrogels before (a) and after (b) deposition of a polyelectrolyte multilayer. Multilayers of chitosan and alginate were deposited (a-b) on hemi-ellipsoidal ionic hydrogels covalently attached to an optical fiber. The optical length of the hydrogels were determined using an interferometric readout platform where information related to changes of hydrogel swelling were deduced from the net interference wave of the incident wave-packet (λ_a - λ_b in the infrared region) reflected at the fiber hydrogel (R1) and hydrogel immersion solution (R2) interfaces (e). Fitting of the constraining effect of the multilayer on the experimentally determined swelling of the ionic hydrogel (□ symbols) by finite element modeling (d) provides information of the mechanical properties of the deposited polymer film when thickness of the film is experimentally determined.

2.2 Fluorescent labeling of chitosan

The chitosan polymer sample was labeled using Alexa Fluor 488 carboxylic acid succinimidyl ester according to the procedure provided by the supplier. Assuming 100% efficiency of the reaction, the mol fraction of amine groups with tagged fluorescence probes was 2.7 mol%. The loss of the reactivity of the reactive dye during packing is $\leq$50% and the reaction efficiency during labeling procedure is about 30-40% (according to the supplier). Thus, the mol fraction of labeled amino groups is reduced from the nominal mixing ratio 2.7 mol%, to around 0.4 mol%.

2.3 Preparation of hydrogels on the optical fibers

Hemi-ellipsoidal hydrogels (radius about 50-60 μm) of co-polymerized AAM and AMPSA were synthesized covalently attached to the end of an optical fiber. Pre-gel solutions composed of 10 wt% of acrylamide, 3 mol% (relative to AAM) of covalent crosslinker, bisacrylamide, and 2.2 mol% of AMPSA were prepared in deionized water. The photoinitiator (hydroxycyclohexylphenyl-ketone) was dissolved in DMSO and added to pre-gel solution to 0.15 mol%. A droplet of the pre-gel solution was deposited at the end of optical fiber immersed in a droplet of squalane. The photoinitiated polymerization was carried out in a squalane solution to avoid evaporation of water during the polymerization. Polymerization was induced by 6 minutes exposure to UV light (Dymax Bluewave 50) using a light guide aligned with the fiber with deposited pre-

gel solution. The optical fiber with the polymerized hydrogel was removed from the squalane and rinsed in excess of 0.15 M NaCl solution in order to remove possible unpolymerized monomers and equilibrate the gel.

2.4 Interferometric monitoring of hydrogel properties

A high resolution interferometric technique (Invivosense) was employed for monitoring the optical length changes of non-modified hydrogel and hydrogel with deposited multilayers upon variation of ionic strength in immersing solution.

The interferometric setup consisted of an optical fiber of diameter $2R_f = 125\mu$m with a hydrogel physically bound at one end and a connector/adapter system at the other (connector: FOC2 STD-A600, Huber + Suhner, adapter: FOC2 FOC2-D001, Huber + Suhner). The optical fiber (108163/02 Huber + Suhner) was connected to the combined light source and detector controlled by a computer employing a LabView program (Invivosense). The hemi-ellipsoidal hydrogel, with radius of about 50-60 μm deposited at the end of the optical fiber, acts as Fabry-Perot cavity for the infrared beam (1530-1560 nm). Both changes in the amplitude and the phase of the reflected interference wave can be employed for monitoring properties of the attached hydrogel[14], however, the changes in the optical length (l_{opt}) of the gel cavity determined based on the change in the phase of the interference wave yields data with the best resolution.[14] Optical length changes are measured with 2 nm resolution and the sample rate is about 1 Hz[14]. Changes in optical length, Δl_{opt} were monitored until the hydrogels reached the new equilibrium swelling volume following ionic strength changes.

2.5 Multilayer deposition and hydrogel characterization

The optical fiber with synthesized hydrogel was kept in glass tubes with an inner diameter of 1 mm filled with 150 mM NaCl solution. Chitosan-alginate mulilayers buildup was carried out from 150 mM NaCl solution at pH$\sim$5.4 after pre-equilibration of the hydrogel. Polymer concentration in the buffer solution was 1 mg/ml. The anionic hydrogel was first exposed to cationic chitosan for 5 min. Before and after deposition of alginate the hydrogel was washed for 10 min. in 0.15 M NaCl. The procedure was repeated up to 12 times. The non-modified hydrogel and the hydrogel with deposited 4 and 8 bilayers were equilibrated in $5 \cdot 10^{-4}$ M NaCl aqueous solution before determining the swelling behavior at increasing ionic strength. The changes in the optical length of the hydrogel, Δl_{opt}, relative to the overall optical length of AMPSA hydrogels l_{opt} measured in 0.5 mM NaCl, were employed as a parameter for changes of the hydrogel swelling.

2.6 Laser scanning confocal microscopy

The middlemost cross-section of hydrogel with deposited multilayers was imaged using confocal laser scanning microscopy (LSM 510 Meta, Carl Zeiss Jena GmbH, Jena, Germany) equipped with an Ar laser and LSM 4.2 software. The cationic chitosan component used in the deposition of the multilayer was labeled with Alexa Fluor 488 dye. The image was acquired using 40$\times$ magnificaton water immersion objective (numerical aperture N.A. = 1.2), excitation wavelength λ_{ex} = 488 nm, a bandpass BP500-550 nm filter in front of the detector, and a pinhole diameter of 94 μm. The multilayer thickness was estimated

as an arithmetic mean value of six FWHM of the peak on fluorescence intensity distribution profiles taken across the hydrogel radius, see below.

2.7 Polymer network elasticity

The behavior of a swollen polymer network and the different free energy densities arising from the different aspects contributing to the swelling phenomenon are presented in this section.

2.7.1 Kinematics

Let Ω_0 and Ω be the reference (dry state) and current configurations, respectively. The deformation map $\varphi(\mathbf{X}) : \Omega_0 \rightarrow \mathbf{R}^3$ transforms a material point $\mathbf{X} \in \Omega_0$ into the related current position $\mathbf{x} = \varphi(\mathbf{X}) \in \Omega$. Therefore, the deformation gradient $\mathbf{F}$ is defined as $\mathbf{F} = \partial\varphi(\mathbf{X})/\partial\mathbf{X} = \partial\mathbf{x}/\partial\mathbf{X}$, with the volume ratio $J = \det\mathbf{F} > 0$. For further use, we introduce an intermediate configuration Ω_1, the deformation gradient of the intermediate configuration Ω_1 relative to the dry configuration Ω_0 $\mathbf{F}_0$ and the deformation gradient of the current configuration Ω relative to the intermediate configuration Ω_1 $\mathbf{F}_1$ (Figure 2). This leads to the following relations:

$$\mathbf{F} = \mathbf{F}_1\mathbf{F}_0, \quad J_0 = \det\mathbf{F}_0, \quad J_1 = \det\mathbf{F}_1, \quad J = J_0J_1. \tag{1}$$

In addition, the right and left Cauchy Green deformation tensors $\mathbf{C}$ and $\mathbf{B}$, respectively, are defined as:

$$\mathbf{C} = \mathbf{F}^T\mathbf{F}, \quad \mathbf{B} = \mathbf{F}\mathbf{F}^T. \tag{2}$$

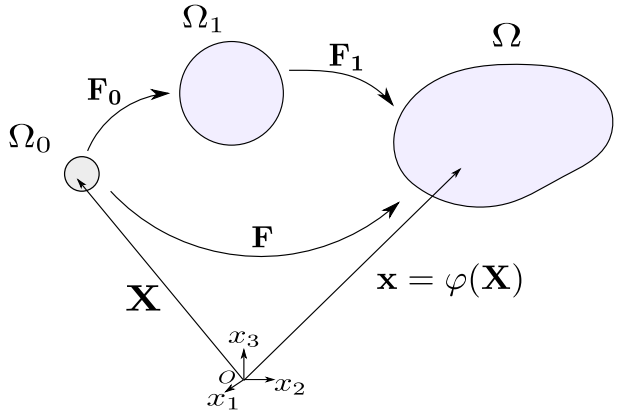

Fig. 2: Configurations: Ω_0 is the reference configuration or dry state, Ω is the current configuration and Ω_1 is an intermediate configuration such that $\mathbf{F} = \mathbf{F}_1\mathbf{F}_0$

2.7.2 Equilibrium conditions

It is first necessary to establish some relations regarding the chemical potential of the diffusible species (Figure 3) and the different ways to express their concentrations. The chemical potential for the different

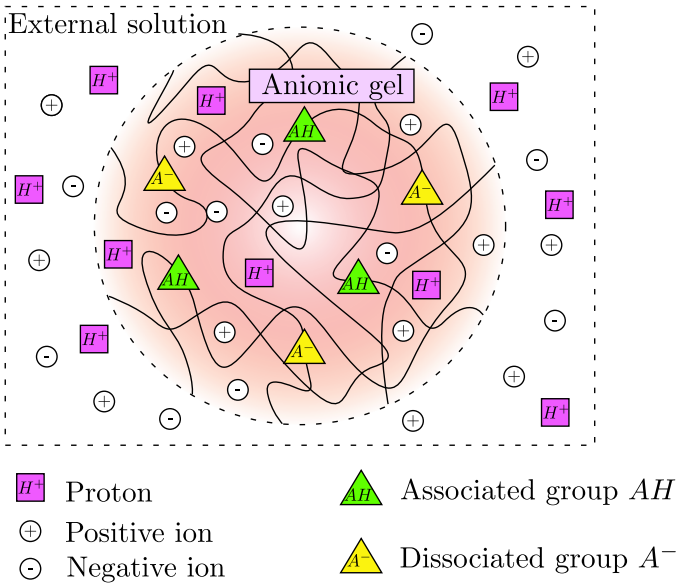

Fig. 3: Anionic polymer network surrounded by an external solution: the polymer network contains fixed ionizable groups and charges and both network and external solution contain the solvent and free ions

mobile species (H^+,+,− see Figure 3), indicated by the subscript, is given by Marcombe et al. and Hong et al.:[12,15]

$$\mu_+ = k_B T \ln\left(\frac{\bar{c}_+}{c_+^{ref}}\right), \tag{3}$$

$$\mu_- = k_B T \ln\left(\frac{\bar{c}_-}{c_-^{ref}}\right), \tag{4}$$

$$\mu_{H^+} = k_B T \ln\left(\frac{\bar{c}_{H^+}}{c_{H^+}^{ref}}\right), \tag{5}$$

where k_B is the Boltzmann constant, T the absolute temperature, $\bar{c}_\alpha$ and c_α^{ref} are the concentration in the external solution and the reference concentration of given species α, respectively.

The chemical potential for the solvent μ_S is given by:

$$\mu_S = -k_B T v_S \sum_{\alpha \neq S} \bar{c}_\alpha, \tag{6}$$

with v_S the volume per solvent molecule. Note that here $v = v_S$, where v is the volume per monomer (see eq.(13)).[12]

The relation between the nominal C_α and true c_α concentration of given species α inside the network is

$$C_\alpha = J c_\alpha, \tag{7}$$

while the relation between the volumetric and molar concentration is

$$c_\alpha = N_A[\alpha], \tag{8}$$

where N_A is Avogadro's number.
We assume that individual polymers and solvent molecules to be incompressible and the volume fraction of the mobile ions to be sufficiently low to neglect their contributions to the volume of the gel. Therefore, taking into account these assumptions the Jacobian of the deformation J reads:

$$J = 1 + v_s C_s. \tag{9}$$

Note that for the dry network $J = 1$. For $v_S C_S \gg 1$ eq.(9) reduces to

$$J \simeq v_S C_S. \tag{10}$$

In an anionic polymer network the following reaction takes place

$$AH \rightleftharpoons A^- + H^+ \tag{11}$$

yielding negatively charged monomer groups upon dissociation. This can be expressed in terms of the acid dissociation constant, K_a:

$$K_a = \frac{[H^+][A^-]}{[AH]}. \tag{12}$$

The total number of ionizable monomer groups is conserved through the relation

$$C_{AH}(\mathbf{X}) + C_{A^-}(\mathbf{X}) = \frac{f}{v}, \tag{13}$$

where f is the fraction of monomers with ionizable groups and v the volume per monomer. The equilibrium conditions are found when the total variation of Helmholtz free energy W of the system is zero:

$$\begin{aligned} \delta W &= \int \delta U dV + \mu_S \delta \bar{n}_S + \mu_{H^+} \delta \bar{n}_{H^+} + \mu_+ \delta \bar{n}_+ + \mu_- \delta \bar{n}_- \\ &\quad - \int B_i \delta x_i dV - \int T_i \delta x_i dS = 0, \end{aligned} \tag{14}$$

where U is the free energy function, δ the variation parameter, $\bar{n}_\alpha$ is the number of given mobile species α, x_i the current coordinates, B_i and T_i the components of the body and traction forces, respectively.
The negative ions, positive ions and solvent molecules do not react chemically with the polymer network, and the total number of free species is thus conserved. The balance of each species across the surface of the network can be expressed as

$$\int \delta C_-(\mathbf{X})\, dV = -\delta \bar{n}_- \tag{15}$$

$$\int \delta C_+(\mathbf{X})\, dV = -\delta \bar{n}_+ \tag{16}$$

$$\int \delta C_S(\mathbf{X})\, dV = -\delta \bar{n}_S. \tag{17}$$

The condition of electroneutrality must be fulfilled both inside and outside the network. In the external solution, the condition can be expressed in terms of the number of each mobile species:

$$\bar{n}_{H^+} + \bar{n}_+ = \bar{n}_-. \tag{18}$$

To express this condition inside the network, together with the conservation of H^+, the fixed charges and the properties of the ionizable monomers in the gel must also be taken into account. The condition of electroneutrality inside an anionic network can be expressed in terms of the concentration of the different charged species present:

$$C_{H^+}(\mathbf{X}) + C_+(\mathbf{X}) = C_{A^-}(\mathbf{X}) + C_-(\mathbf{X}). \tag{19}$$

The conservation of H^+ within the anionic network and across its surface can be expressed as

$$\int \delta C_{H^+}(\mathbf{X})\, dV - \int \delta C_{A^-}(\mathbf{X})\, dV = -\delta \bar{n}_{H^+}. \tag{20}$$

Inserting (19) into (20) gives the following expression for the change in protons in the external solution:

$$\delta \bar{n}_{H^+} = \int \delta C_+(\mathbf{X})\, dV - \int \delta C_-(\mathbf{X})\, dV = \delta \bar{n}_+ - \delta \bar{n}_- \tag{21}$$

Now using eq.(9) and eqs.(15-21), the equilibrium condition of the system eq.(14) becomes:

$$\begin{aligned} \delta W \;=\; & \int \delta U dV - \int \frac{\mu_S}{v_s} \delta J(\mathbf{X})\, dV - \int (\mu_+ - \mu_{H^+}) \delta C_+(\mathbf{X}) dV - \int (\mu_- - \mu_{H^+}) \delta C_-(\mathbf{X}) dV \\ & - \int B_i \delta x_i dV - \int T_i \delta x_i dS = 0. \end{aligned} \tag{22}$$

2.7.3 Free energy function U for hydrogel

In order to describe the mechanical behavior of the anionic gel used in this study, we use the following free energy function U consisting of four parts:

$$U = U_{str} + U_{mix} + U_{ion} + U_{dis}. \tag{23}$$

U_{str} represents the free energy of stretching per volume of the polymer chains and is given as[15–17]:

$$U_{str} = \frac{1}{2} N k_B T \left(I_1 - 3 - 2\ln(J) \right), \quad \text{with } I_1 = \mathrm{tr}\mathbf{C}, \tag{24}$$

with N the network crosslink density. U_{mix} represents the free energy of mixing of the polymer network and the solvent[16,18]:

$$U_{mix} \;=\; \frac{k_B T}{v_s} \left(v_s C_s \ln\left(\frac{v_s C_s}{1 + v_s C_s} \right) + \chi \left(\frac{v_s C_s}{1 + v_s C_s} \right) \right), \tag{25}$$

which becomes using eq.(9),

$$U_{mix} \;=\; \frac{k_B T}{v_s} \left((J-1) \ln\left(1 - \frac{1}{\mathrm{J}} \right) + \chi \left(1 - \frac{1}{\mathrm{J}} \right) \right), \tag{26}$$

where χ is the Flory-Huggins parameter,
The free energy of mixing of the mobile ions U_{ion} is given by Hong et al.[19]:

$$U_{ion} = k_B T \sum_{\alpha \neq s} C_\alpha \left(ln \frac{C_\alpha}{v_s C_s c_\alpha^{ref}} - 1 \right), \tag{27}$$

which becomes using eq.(10),

$$U_{ion} = k_B T \sum_{\alpha \neq s} C_\alpha \left(ln \frac{C_\alpha}{J c_\alpha^{ref}} - 1 \right). \tag{28}$$

The free energy of dissociation U_{dis} can be expressed as[12,18]:

$$U_{dis} = k_B T \left(C_{AH} \ln \left(\frac{C_{AH}}{C_{A^-} + C_{AH}} \right) + C_{A^-} \ln \left(\frac{C_{A^-}}{C_{A^-} + C_{AH}} \right) \right) + \gamma C_{A^-}, \tag{29}$$

with γ the molar heat of dissociation.
Finally, the free energy of the gel is a function of $\mathbf{C}$, C_{H^+}, C_+, C_-:

$$U = U(\mathbf{C}, C_{H^+}, C_+, C_-). \tag{30}$$

2.7.4 Cauchy stress tensor and initial state

Taking into account the balance of species across the surface of the hydrogel network, electroneutrality both in the gel and in the external solution and eq.(9), the equilibrium condition (eq.(22)) of the system consisting of the gel and the external solution at constant temperature leads to the following expression for the Cauchy stress tensor σ[12]

$$\sigma = \frac{N k_B T}{J} (\mathbf{B} - \mathbf{1}) + p\mathbf{1}, \tag{31}$$

$$\text{with} \quad p = -kT \left(c_{H^+} + c_+ + c_- - \bar{c}_{H^+} - \bar{c}_+ - \bar{c}_- \right) + \frac{kT}{v_s} \left(\ln \left(\frac{J-1}{J} \right) + \frac{\chi}{J^2} + \frac{1}{J} \right). \tag{32}$$

In addition, three equations are derived from the equilibrium condition of the system: the Donnan equations,

$$\frac{c_+}{\bar{c}_+} = \frac{c_{H^+}}{\bar{c}_{H^+}} \quad \text{and} \quad \frac{c_-}{\bar{c}_-} = \frac{\bar{c}_{H^+}}{c_{H^+}} \tag{33}$$

and the condition of chemical equilibrium,

$$\frac{c_{H^+}(c_{H^+} + c_+ - c_-)}{\frac{f}{vJ} - (c_{H^+} + c_+ - c_-)} = N_A K_A \quad \text{with} \quad N_A K_A = c_{H^+}^{ref} exp(-\frac{\gamma}{kT}). \tag{34}$$

The system of eqs.(33-34) can be solved to express the ion concentrations c_{H^+}, c_+ and c_- inside the hydrogel as functions of the ion concentrations $\bar{c}_{H^+}$, $\bar{c}_+$ and $\bar{c}_-$ in the external solution and J.
In this study, all the finite element analyses start in an intermediate configuration Ω_1 (see Figure(2)) where the gel is stress free and in a state of isotropic strain: $\mathbf{F}_0 = \lambda_0 \mathbf{1}$ and $J = \lambda_0^3$. λ_0 is found by solving numerically $\sigma(\lambda_0) = \mathbf{0}$ for given $\bar{c}_{H^+}$, $\bar{c}_+$ and $\bar{c}_-$.

2.7.5 Constitutive model for the multilayers

Although prepared by a sequential deposition process, polyelectrolyte multilayers in general show large degree of interprenetation between the various components.[20] As a first approximation, it is assumed that also the multilayer deposited on the hydrogel shows similar degree of interprenetation, and for this reason, the shell is modeled as only one material. Finite extensibility of the polymers within the shell can be implemented using e.g. inverse Langevin approximation[21,22] or other models.[23] The average mechanical behavior of the multilayers is modeled with the following strain energy W function proposed by Ehret and Böl[23] for biofilms,

$$W = \frac{C_0}{4}\Omega\left(\frac{1}{1-\Lambda\sqrt{I_1/3}} - \Lambda\left(\sqrt{\frac{I_1}{3}} - 2\Lambda\frac{I_1}{3} + \Lambda^2\left(\frac{I_1}{3}\right)^{3/2}\right)\right) + W_0, \tag{35}$$

$$\text{with} \qquad \Omega = \frac{L}{l_p}, \quad \Lambda = \frac{r_0}{L} \quad \text{and} \quad r_0^2 = 2l_p^2\left(\frac{L}{l_p} - 1 + e^{-L/l_p}\right), \tag{36}$$

where L is the contour length, l_p the persistence length and r_0 the end-to-end distance between two junctions in the reference configuration. W_0 is a constant term calculated such as $W(I_1 = 3) = 0$. C_0 is a material parameter to be determined in the present study representing the equivalent elastic properties of the chitosan-alginate multilayers. The multilayers are modeled as fully incompressible. Note that results accounting for mixing of the solvent with the multilayers are presented in the supplementary material. The constitutive material model defined by eq.(35) was implemented in an ABAQUS user-subroutine UHYPER.

2.8 Finite element models

Two finite element models (models 1 and 2) are used in this study (see Figure(4)). Model 1 and model 2 correspond to the anionic gel without ($t = 0$) and with ($t \neq 0$) polymer coating, respectively, and are used to determine by means of an inverse modeling technique (detailed in section 2.9) the network crosslink density N and the Flory-Huggins parameter χ of the anionic gel and the elastic property C_0 of the shell, respectively.

The hydrogel which has the shape of a hemi-ellipsoid with height L_g is bound to an optical fiber of diameter $2R_f = 125\mu m$. The polymer coating is modeled by a thin layer (in red in Figure(4)) of thickness t.

The height of the hydrogel at a salt concentration of 0.15 M is denoted $L_{g,0.15}$ and is taken as the height of the hydrogel in Ω_1 the stress free configuration.

Both models are axisymmetric. Therefore, the hydrogel is modeled with a quarter of an ellipse. The geometry is meshed with eight noded axisymmetric elements with reduced integration (CAX8RT ABAQUS type). The nodes on the bottom edge in Figure(4) are constrained in all directions to represent the boundary conditions with the optical fiber assumed to be rigid.

All the analyses are performed using ABAQUS/Standard with a fully coupled temperature-displacement procedure. The salt concentration in the external solution $\bar{c}_+$ is imposed as a temperature boundary condition on the gel and the shell. The pH ($\bar{c}_{H^+} = 10^{-pH}$) is assumed to be constant and equal to 5. This value, close to the experimental conditions (pH$\sim$5.4), is chosen to improve numerical convergence.

To simulate the material behavior of the gel and the shell, the UHYPER user-subroutine provided by Marcombe et al.[12] was used. We modified it in order to be able to impose the salt concentration ($\bar{c}_+$) as a

boundary condition. Therefore, the AMPSA gel is modeled as an anionic gel sensitive to the pH and the salt concentration in the external solution. The shell (chitosan-alginate) is assumed to be a neutral gel that is insensitive to the mobile ions in the external solution.

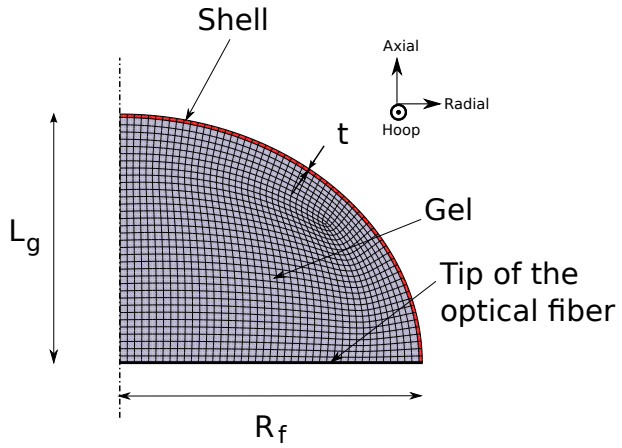

Fig. 4: Finite element models. Model 1 corresponds to the anionic gel without polymer coating ($t = 0$). Model 2 corresponds to the anionic gel with polymer coating ($t \neq 0$).

2.9 Identification of the material parameters

The network crosslink density N and the Flory-Huggins parameter χ of the hydrogel (AMPSA) used in this work were unknown. We identified the two parameters N and χ by fitting the length of the hydrogel sensor L_g^{FE} (model 1, see section 2.8) computed using the finite element software ABAQUS to the length L_g^{exp}. L_g^{exp} was measured during our swelling experiment with varying salt concentration (varying $\bar{c}_+$) and constant pH (constant $\bar{c}_{H^+}$) and the hydrogel bound to the optical fiber without deposited polymer layer. The fitting was performed using the *lsqnonlin* function in the Optimization Toolbox of the commercial software Matlab together with the trust-region-reflective algorithm. Therefore, the fitting of N and χ consists in minimizing the following nonlinear function,

$$S = \sum_{i=1}^{n} \left(\frac{L_{g,i}^{FE} - L_{g,0.15}^{FE}}{L_{g,0.15}^{FE}} - \frac{L_{g,i}^{exp} - L_{g,0.15}^{exp}}{L_{g,0.15}^{exp}} \right)^2, \tag{37}$$

where n is the number of data points corresponding to different salt concentration levels in the external solution $\bar{c}_+$. The numerical procedure is summarized in Figure 5.

Then, the material parameter C_0 in eq.(35) of the thin polymer layer deposited on the surface of the ionic hydrogel is determined using a similar numerical procedure and using the network crosslink density N and the Flory-Huggins parameter χ for the ionic hydrogel found previously and the finite element model 2 , see Figure(4). Two types of polymer coating are used in this study with 4 and 8 bilayers (Chitosan-alginate), respectively. Therefore, C_0 is calculated for these two thin polymer films.

Require: : initial set of parameters $\{N_0\ ,\ \chi_0\}$ and $L_{g,i}^{exp}$ for i=1..n
k=0
while $S > tol$ **do**
compute λ_0 corresponding to $\{N_k\ ,\ \chi_k\}$
compute $L_{g,i}^{FE}$ for i=1..n with ABAQUS using the set of parameters $\{N_k\ ,\ \chi_k,\ \lambda_0\}$
compute S
compute a new set of parameters $\{N_{k+1}\ ,\ \chi_{k+1}\}$ with *lsqnonlin*
k=k+1
end while
return $N = N_k$ and $\chi = \chi_k$

Fig. 5: Algorithm to estimate N and χ by means of nonlinear least square technique

3 Results and discussion

3.1 Multilayer thickness

Confocal micrographs of the hydrogel with deposited eight chitosan/alginate bilayers show significantly higher fluorescence intensity at the hydrogel surface comparing to hydrogel interior (Figure 6). This suggest that fluorescently labeled chitosan is mainly deposited at the hydrogel surface and most likely only lower molecular weight fractions of the polymer diffused toward the interior contributing to slight fluorescence from the hydrogel bulk. The experimentally determined optical length and changes in this associated with

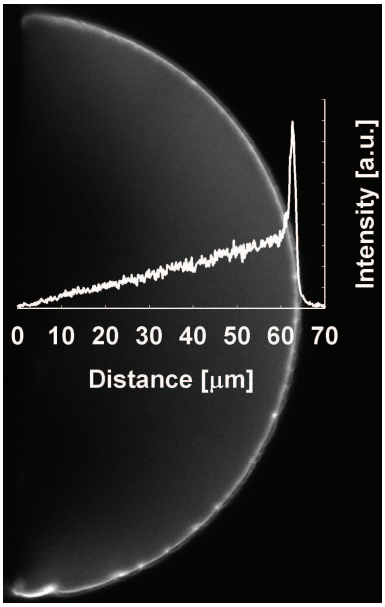

Fig. 6: Confocal laser scanning microscopy image of the middlemost cross section of AMPSA hemi-ellipsoidal hydrogel core attached to optical fiber with deposited 8 chitosan/alginate bilayers. Image was taken after hydrogel equilibration in aqueous 0.5 mM NaCl solution.

13

swelling was converted to physical length based on our previous approach.[14,24,25] In general, the net change in Δl_{opt} can arise both due to altered optical properties or changes in physical length of the hydrogel,

$$\Delta l_{opt} = \langle n_2 \rangle l_2 - \langle n_1 \rangle l_1 \simeq \langle n_1 \rangle \Delta l + l_1 \Delta n, \tag{38}$$

where subscripts 1 and 2 represent the two states to be compared, and

$$\langle n_i \rangle = l_i^{-1} \int_0^{l_i} n_i(l) \mathrm{d}l, \quad i = 1,2, \tag{39}$$

are the average of the refractive indices along the optical pathway of the two states. For the ionic strength induced hydrogel swelling, the major contribution is from the change in the physical length, and the associated change in concentration of the polymer does not affect the optical properties of the hydrogel substantially.[14] Thus, the physical length is obtained by dividing the optical length by a constant refractive index. Note also that for the changes in physical length is reported to be the dominating contribution to Δl_{opt} in cases of interpenetrating materials.[24,25]

The resolution in the confocal microscope does not allow resolving any major difference between the four and eight chitosan-alginate bilayer although such a difference could be expected based on influence of number of deposition cycles for multilayers prepared on solid substrates. In case of multilayers deposited on a modified polystyrene surfaces the average thickness increment per one chitosan-alginate bilayer was around 4-6 nm.[26] Multilayer buildup up to 4 and 8 bilayers is thus expected to result in around 16-24 and 32-48 nm total thickness. The thickness difference between 4 and 8 bilayers in such a system is far below the confocal microscopy resolution limits. When the cationic polymer is deposited at the porous anionic hydrogel surface one can expect more pronounced penetration of at least first layer into the substrate. The penetration depth is dependent on the molecular properties of both substrate and the impregnating polymer.[24] The confocal image shows that the penetration depth of the polymer is not larger than 0.8 μm for both four and eight chitosan-alginate bilayers. This value is used in the finite element analyses to estimate the elastic parameter C_0 by means of nonlinear-least-square technique and we discuss the implications of using higher resolution data for thin film thickness estimates.

3.2 Crosslink density, Flory-Huggins parameter and elastic property of the multilayers

The identified material parameters obtained with the FE constrained model for the ionic hydrogel (AMPSA) and the deposited shells with 4 and 8 bilayers (Chitosan-alginate) are summarized in Tables 1 and 2. In these models, a persistence length of $l_p = 15$ nm was selected based on the reported data for alginate.[27] An upper bound of the L parameter was estimated to 250 nm based on the molecular mass of the the employed alginate, and effects of smaller spacing between crosslinking points were assessed (see below). Comparisons between experiments and numerical simulations using the identified parameters, provided in Figure 7, show satisfying agreement.

The material constant $C = 1/2Nk_BT$ in front of the Neo-Hookean term in eq.(24) is linearly dependent on the crosslink density N, thus the crosslink density characterizes the elastic properties of the network.

Table 1: Parameters of the ionic hydrogel (APSMA)

	vN	χ	pKa	f	t	$L_{g,0.15}^{exp}$
AMPSA	3.3e-3	0.48	2.0	0.022	0	54.0 μm
$SO_3H \rightleftharpoons SO_3^- + H^+$						

Table 2: Elastic parameter C_0 (eq.(35))for the deposited shells with 4 and 8 bilayers (Chitosan-alginate)

		$C_0/(k_BT/v)$	l_p	L	t	$L_{g,0.15}^{exp}$
Chitosan-alginate	4 bilayers	2.1e-2	15 nm	250 nm	0.8$\pm$0.2 μm	54.7 μm
	8 bilayers	2.6e-2	15 nm	250 nm	0.8$\pm$0.2 μm	50.2 μm

Using $v = 10^{-28}\,\mathrm{m}^3$ and $T = 295$ K, C is equal to 0.067 MPa for the AMPSA gel.
In the case of $l_p << L$ and moderate value of I_1 (here $I_1 < 4$), which is the case for the results reported in Table 2, the material response described by the strain energy function W is very close to the Neo-Hookean one[23]. Therefore, the value of $C_0/2$ can be used for comparison with the elastic property C of the gel. In Table 2 $C_0/2$ is equal to 0.43 MPa and 0.52 MPa for the four and eight bilayers thin films, respectively. Additionally, the reported values of C_0 in the supplementary material when mixing of the solvent with the multilayer shell is accounted for are slightly lower.
Therefore, the deposited shells are substantially stiffer than the AMPSA gel. In addition, the values of the elastic moduli of the multilayers obtained here are slightly higher than the values measured using nanoindentation technique for crosslinked chitosan-hyaluronan multilayers.[28]
The elastic properties of the four and eight multilayers are difficult to compare given the uncertainty of the thickness measure as discussed in Section 3.1. One could expect that the eight bilayer shell to be thicker than the four bilayer one. Therefore, two additional analyses were performed to determine the elastic property of the four bilayers assuming the shell thickness equal to 0.6 and 0.7 μm. The results are summarized in Table 3. The results from Table 3 show as expected that when the shell thickness decreases the calculated

Table 3: Elastic parameter C_0 (eq.(35))for the deposited shells with 4 bilayers (Chitosan-alginate) for assumed thicknesses of 0.6, 0.7 and 0.8 μm

		$C_0/(k_BT/v)$	l_p	L	t	$L_{g,0.15}^{exp}$
Chitosan-alginate	4 bilayers	2.9e-2	15 nm	250 nm	0.6 μm	54.7 μm
	4 bilayers	2.4e-2	15 nm	250 nm	0.7 μm	54.7 μm
	4 bilayers	2.1e-2	15 nm	250 nm	0.8 μm	54.7 μm

value of C_0 increases and when the thickness is reduced from 0.8 to 0.7 μm the stiffness of the four bilayer shell is very close to the one of the eight bilayer shell of thickness 0.8 μm (see Table 2). This may suggest that eight and four bilayer shells have essentially the same stiffness.
Changes of ionic strength is well known to affect the persistence length of polyelectrolytes.[27,29–32] Although the decrease of NaCl is expected to increase the chain stiffness of the alginate and chitosan used in the preparation of the film, such an increase is less than expected from dilute solution estimates because of the multilayer state. The ionic strength that alginate polymer experiences in the multilayer is different from the ionic strength present in the external bath. In order to estimate the polymers contribution to the net ionic

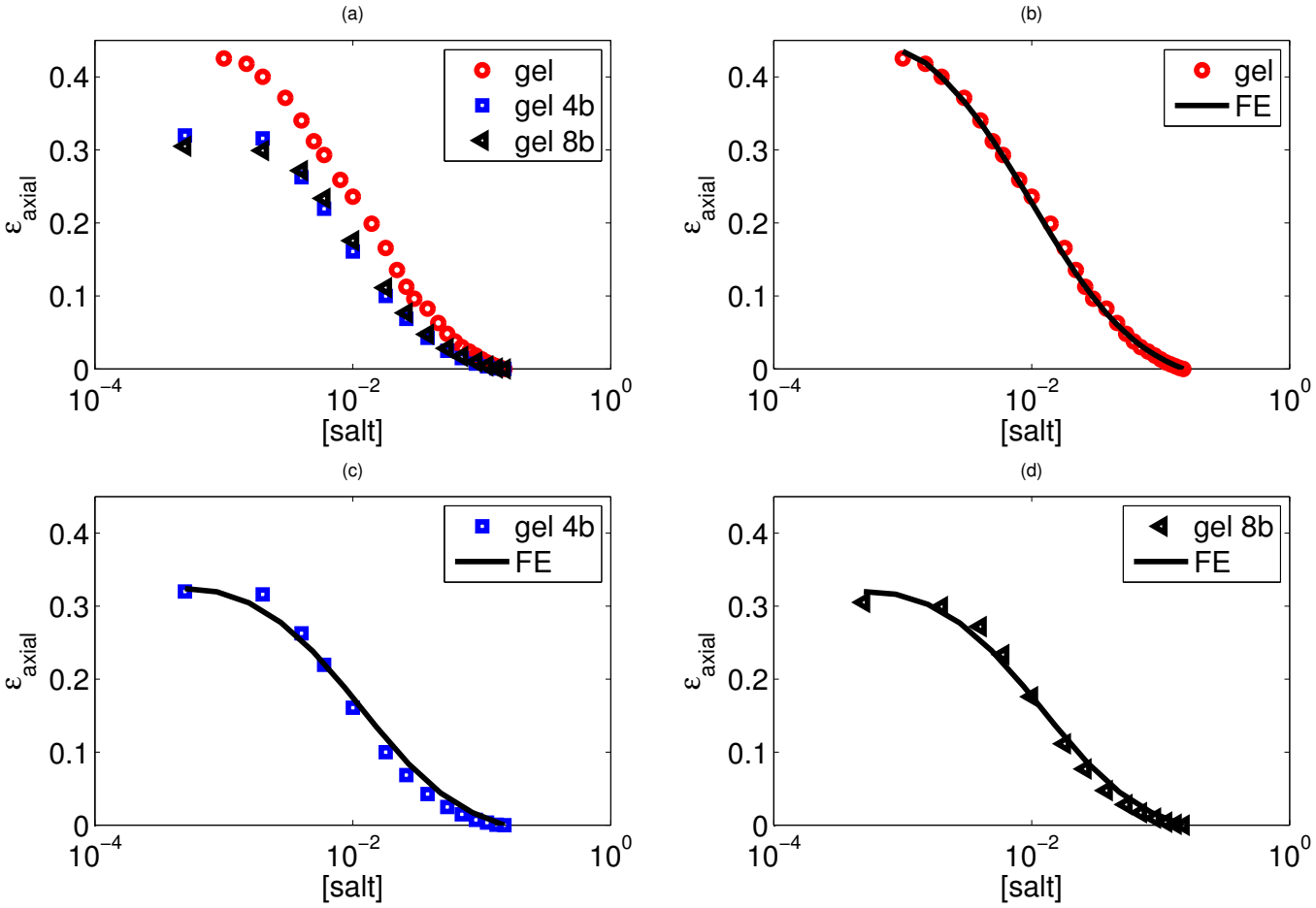

Fig. 7: Comparison between the axial strain ε_{axial} (eq.(40)) of the hydrogel measured during experiments at different levels of salt concentration and the one computed from finite element analyses with the fitted parameters from Tables 1 and 2. Red circles, blue squares and black triangles correspond to experimental results for the gel without deposited layer, the gel with four and eight bilayer chitosan-alginate coating, respectively. The solid lines correspond to the numerical results. a) Experimental results. b), c) and d) comparison between experimental results and numerical analyses for the gel without deposited layer, the gel with four and eight bilayer coating, respectively.

strength in the multilayer the quantitative study on the polymers adsorption would be required.
In order to address this issue, we performed a sensitive study on the ratio Ω in eq.(36), results are reported in Table 4. The results from Table 4 show that when $\Omega < 10$ the computed value C_0 decreases significantly. However, when $\Omega \geq 10$ (i.e. material response close to the Neo-Hookean one), the obtained values of C_0 are somewhat in the same range.

Table 4: Elastic parameter C_0 (eq.(35))for the deposited shells with 8 bilayers (Chitosan-alginate) for different values of the contour length L

		$C_0/(k_BT/v)$	l_p	L	Ω	t	$L^{exp}_{g,0.15}$
Chitosan-alginate	8 bilayers	4.3e-3	15 nm	15 nm	1	0.8 μm	50.2 μm
		1.4e-2	15 nm	45 nm	3	0.8 μm	50.2 μm
		1.9e-2	15 nm	75 nm	5	0.8 μm	50.2 μm
		2.4e-2	15 nm	150 nm	10	0.8 μm	50.2 μm
		2.5e-2	15 nm	225 nm	15	0.8 μm	50.2 μm
		2.7e-2	15 nm	450 nm	30	0.8 μm	50.2 μm
		2.8e-2	15 nm	>900 nm	>60	0.8 μm	50.2 μm

3.3 Comparison between constrained and free swelling

To investigate the influence of the boundary condition between the hydrogel and the optical fiber on the global response, two analyses are performed with model 1 (Figure 4) using the fitted parameters for the AMPSA gel reported in Table 1 for the hydrogel. One analysis had the nodes along the tip of the optical fiber constrained in every directions (constrained case) corresponding to the experimental implementation with the hydrogel covalently attached to the end of the optical fiber. It is compared with a second one where the displacement of these nodes in the radial direction is allowed (free swelling, i.e. stress free). The axial strain defined as

$$\varepsilon_{axial} = \frac{L_g - L_{g,0.15}}{L_{g,0.15}}, \tag{40}$$

and the volumetric ratio $\frac{V}{V_0}$, where V and V_0 are the volumes of the hydrogel in the current and dry configurations, respectively, are plotted against the salt concentration in Figure 8 for both cases. Note that here $L_{g,0.15}$ is identical for the constrained and free swelling cases.
Figure 8 shows the same trends for ε_{axial} and $\frac{V}{V_0}$ in both cases. Additionally, the constraint reduces the swelling $\frac{V}{V_0}$ but increases ε_{axial} in comparison with the free swelling case. These results are in agreement with previous studies.[12,19,33]
Due to the constraint in the radial direction along the optical fiber, the hydrogel can not expand as much as in the unconstrained case in this direction. This seems to be balanced by a larger stretching of the gel in the axial direction.
The boundary conditions imposed in this study reduces the total volumetric swelling but promotes swelling in the axial direction. This emphasizes the need of using numerical techniques such as the finite element method to simulate swelling of hydrogels under geometric constraints imposed during experiments.

3.4 Shell effect

The depositions of the four and eight bilayer shells reduce the axial strain ε_{axial} (eq.(40)) of the hydrogel, see Figure 7. At a salt concentration of 10^{-3} M, ε_{axial} is reduced by 23% and 28% for the four and eight bilayers, respectively, compared to the case without coating.
In order to investigate this swelling reduction phenomenon, 900 analyses were performed with 30 different

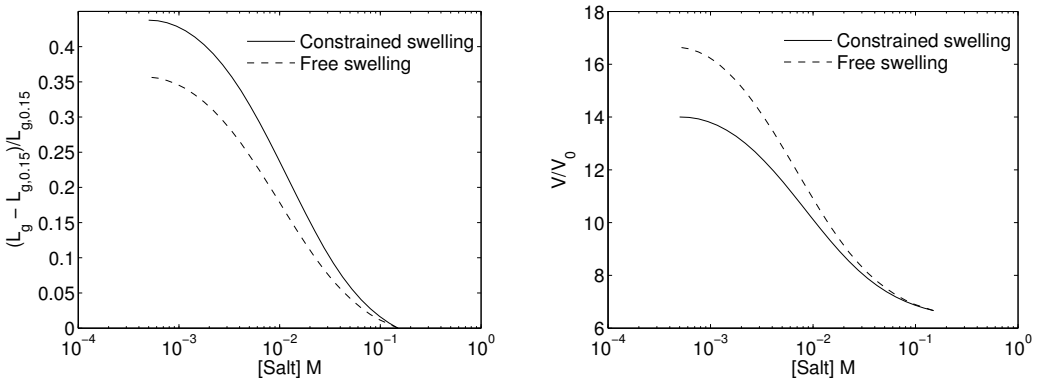

(a) (b)

Fig. 8: Comparison between free and constrained deformations for model 1 (without shell) using the fitted parameters reported in Table 1 for the hydrogel. The solid lines represent the constrained gel bound to the optical fiber and the dashed lines the correspond to free swelling. (a) Axial strain ε_{axial} (eq.(40)), (b) volumetric ratio V/V_0

values of the crosslink density of the shell and 30 values for the shell thickness t using model 2. The parameters reported for the AMPSA gel in Table 1 were used for the hydrogel while 30 values of $\log(C_0/(k_BT/v))$ between -3 and -1 and 30 values of t between 0.27μm and 2.7μm were used for the deposited shell. l_p and L are assumed to be constant and equal to 15 nm and 250 nm, respectively.
The axial strain ε_{axial} of the hydrogel is plotted against $\log(C_0/(k_BT/v))$ and $\frac{t}{L_{g,0.15}}$ at a salt concentration of $5 \cdot 10^{-4}$ M in Figure 9. As can be seen from Figure 9, ε_{axial} decreases when the thickness t of the deposited shell increases and when the elastic property C_0, i.e. the stiffness, of the shell increases.
Figure 8 indicates that ε_{axial} is equal to 0.44 at salt concentration of $5 \cdot 10^{-4}$ M in the constrained case without shell. In addition, Figure 9 shows that when $C_0/(k_BT/v)$ for the shell and the crosslink density the hydrogel have the same order of magnitude ($\log(vN)$=10^{-3}), ε_{axial} is in a range between 0.40 and 0.43 depending on the value of t. This suggests that when the shell's stiffness is slightly above the one of the hydrogel core, the effect of the deposited layer on the reduction of ε_{axial} is diminished.
In addition, this type of contour plot can be used to estimate an equivalent elastic property of a deposited layer assuming that thickness of the shell and the axial strain of the gel can be determined experimentally. This is illustrated in Figure 9 by the horizontal and vertical lines: when for example $t/L_{g,0.15} \simeq 1.3\%$ and $\varepsilon_{axial} = 35\%$ are known from experimental measurements, the elastic property of the shell can be deduced from the graph, in this example we obtain $C_0/(k_BT/v) \simeq 0.018$. Thus, experimental measurements of the reduction of the swelling capacity due to polymer coating and coating thickness can be used for the determination of the deposited film mechanical stiffness. Nevertheless, the presision in this estimate is strongly dependent on the quality of the two experimental data.

The logarithmic strains in the axial, radial and hoop directions are plotted on the deformed shape of the hydrogel with an eight bilayer deposited shell at a salt concentration of $5 \cdot 10^{-4}$ M in Figure 10. As can be seen from the figure, both the AMPSA gel and the chitosan-alginate deposited layer undergo an anisotropic state of strain. However, while the hydrogel experiences tensile strains only, the shell is under compression in the direction perpendicular to its mid-surface.
The deposited shell is modeled, herein, as a neutral gel insensitive to the mobile ions in the external solution

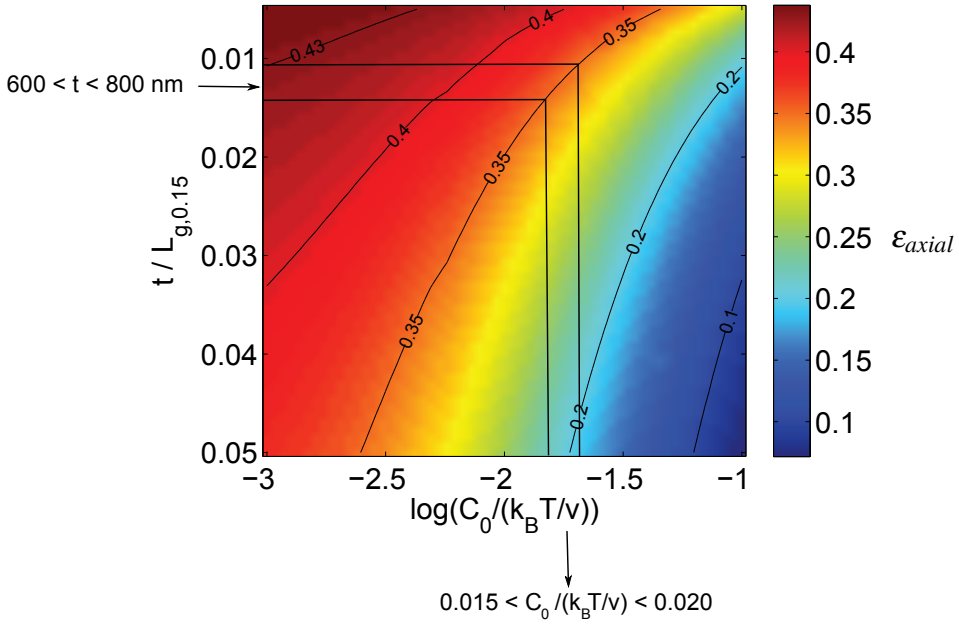

Fig. 9: Color plot of ε_{axial} (eq.(40)) of the hydrogel with deposited layers at a salt concentration of $5 \cdot 10^{-4}$ M for different values of C_0 (eq.(35)) and thickness of the shell. The horizontal and vertical lines illustrate how to read the elastic property of the shell when the thickness and the axial strain are know (here $1.09 < t/L_{g,0.15} < 1.46\%$ and $\varepsilon_{axial} = 35\%$ are known and we read $C_0/(k_B T/v) \simeq 0.018$ for the shell).

while the hydrogel is swelling in response to the decrease in salt concentration. Additionally, the swelling property of the hydrogel is isotropic. Therefore, the chitosan-alginate layer behaves as a membrane subjected to an internal pressure.

In the present approach, a proof of concept experimental realization is analyzed in view of the finite element modeling of thin polymer film layer constraining of ionic hydrogel swelling. Obviously, possible experimental realizations of experiments that can be analyzed following the overall strategy can be extended with respect to molecular parameters of the ionic hydrogel, as well as range of mechanical properties of the deposited polymer films. In the following, some aspects of these parameters are discussed, however, without an experimental counterpart. The crosslink density of the ionic hydrogel as e.g. varied by the molar ratio of BIS relative to AAM in the present case, can experimentally be varied in a large range. However, to be able to observe a constraining effect in the ionic strength induced swelling due to a deposited polymer film, the elastic properties of the deposited layer need to constrain the swelling. Thus, less elastic films is expected to require less densely crosslinked ionic hydrogels to be able to see such an effect. In a previous publication, we compared the swelling response of poly-l-lysine coated alginate hydrogel with the uncoated hydrogel.[34] The finding of no overall constraining in that example is at variance with the constraining observed in the present data (Figure 7). Thus, not all impregnation processes does not necessary lead to a constraining of the hydrogel that can be used as a basis for estimating the mechanical properties of the film as outlined here.

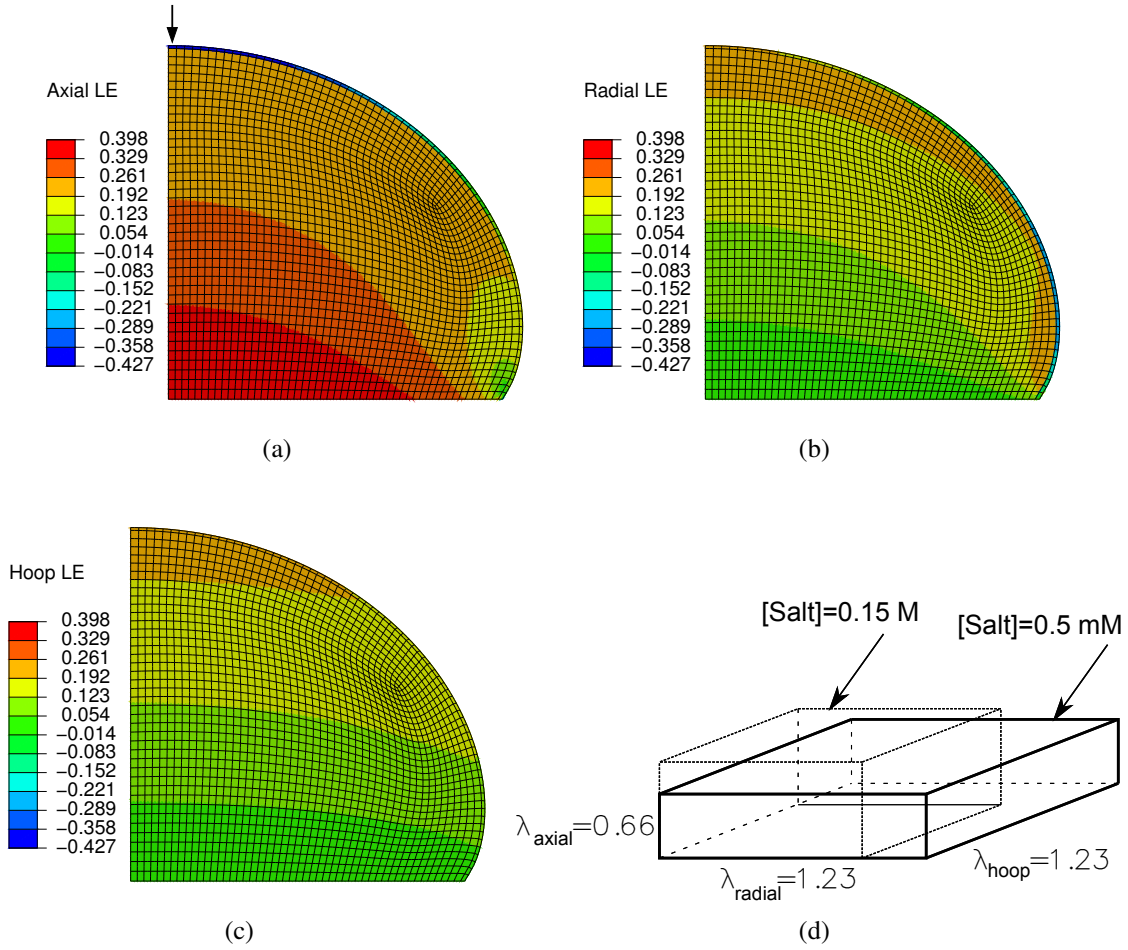

Fig. 10: Logarithmic strains in the (a) axial, (b) radial and (c) hoop directions for the hydrogel with the eight bilayer chitosan-alginate coating at a salt concentration of 0.5 mM. (d) Schematic representation of the stretching of the shell located at the top of the hydrogel as indicated by the arrow in (a).

4 Concluding remarks

This work advances the knowledge of material properties of thin polymer films. We develop a method to characterize multilayer thin films material properties from finite element analysis. Experimental measurements of the deformations of the hydrogel and the thickness of the deposited thin film are used as inputs to determine the crosslink densities of the hydrogel first and the elastic property of deposited multilayer in a second step. This can be achieved by means of an inverse modeling approach using a nonlinear least square technique.

The optical length of the hydrogel can be measured with high precision. However, a somewhat large uncertainty remains in the measurement of the thickness of the deposited layer. In that case an approximated value of the thin layer crosslink density can be determined from a calibration graph such as the color plot in Figure 9. Even though 900 analyses are needed herein to produce such a plot, the computational cost is quite low since the CPU time for one analysis is approximatively 10 s on a 2.5 GHz Intel Core T9300 CPU.

The method described in this work is applied to a hemi-ellipsoidal hydrogel with chitosan and alginate multilayers. It may easily be employed with other types of geometries and polymer films. Therefore, this method can be adapted to the experimental set-up available. Moreover, the numerical method described in this study may be used with other kinds of constitutive material models.

The charge density of the ionic hydrogel is another parameter to consider. This parameter, in combination with total polymer network concentration and crosslink density, affects the swelling ratio between the low and high ionic strength solution,[35–37] and therefore affects the maximum deformation ratios that one can impose on the deposited thin film. In this work, the model for elasticity of the thin film is implemented with standard rubber like elasticity. By varying the charge density of the ionic hydrogel, experimental testing of possible effects of maximum deformation ratio on the obtained properties of the deposited thin film are accessible. In the proof of concept experiments included here, the charge density of the ionic hydrogel is also a key parameter in the deposition of the first polycation layer. Too low charge density of the ionic hydrogel in this experimental line is expected to increase the possibility for (partial) polycation penetration into the hydrogel yielding an overall (partial) polyampholyte character of the ionic hydrogel core. In such cases, as e.g. also reported previously,[24] the current modeling approach needs to be elaborated to reflect the altered nature of the material.

Hydrogels, either as unsupported entities or integrated as a part of layered structures with different mechanical properties, are reported to display formation of creases or buckling patterns.[9,38–40] In the present modeling approach, such effects have not been included. Our approach is thus limited to cases where uniform deformation of the coupled layer is achieved, and the selection of molecular parameters for the ionic hydrogel core offers a range of final properties that can be explored in such a context. Formation of creases or buckles violates not only the assumptions used in the current model, but may also affect the precision of the measurements by making a less smooth interface for the reflection of the incident wave at the thin film layer immersing solution interface.

The total optical length changes measured upon [NaCl] variation from 0.5 mM to 0.15 M in two consecutive tests, showed the same value (data not shown). This suggests that there is no desorption of polymers from the multilayer during swelling tests within the studied concentration range. The reversibility of the optical length changes was tested by subjecting the multilayered hydrogel to increasing and descending [NaCl] changes. Both tests showed the same total optical length changes.

In the proof-of-concept experiments included here, we have studied the effect of constraining of the ionic hydrogel by a deposited multilayer (4 and 8 bilayers) of chitosan and alginate. As a first approximation to include the constraining effect of this thin film (relative to the overall size of the hydrogels), we assumed that these multilayers could be represented as a net uncharged material in the modeling. This assumption was stimulated by the zone model for growth of multilayer. At extended number of deposition cycles, this model describes a middle zone being charge-balanced by the polyanion and polycations, and that this middle zone is embedded between a zone close to the substrate and outermost layer.[20,41] While the outermost zone is visualized as being charged reversed in every polyanion/polycation deposition step, the growth of the multilayer is suggested to occur through the increase of the net neutral zone II. Although the details of the multilayer structure would indicate that a more elaborate representation is needed to take into account detailed features of the multilayers on the constraining of ionic hydrogel swelling, the main part of these structures within the body of the multilayers is net neutral. In such a perspective, our assumption of a net neutral electrostatic polymer hydrogel film appears to be a reasonable assumption, and thus, the derived mechanical properties of the films are representing the actual material properties.

Acknowledgment

This work was supported by the Norwegian Research Council, contract number 191818/V30.

References

1 C. D. Jones and L. A. Lyon, *Macromolecules*, 2003, **36**, 1988–1993.

2 E. Costa, M. M. Lloyd, C. Chopko, A. Aguiar-Ricardo and P. T. Hammond, *Langmuir*, 2012, **28**, 10082–10090.

3 M. Lanniel, E. Huq, S. Allen, L. Buttery, P. M. Williams and M. R. Alexander, *Soft Matter*, 2011, **7**, 6501–6514.

4 S. Yamanlar, S. Sant, T. Boudou, C. Picart and A. Khademhosseini, *Biomaterials*, 2011, **32**, 5590 – 5599.

5 H. Bysell and M. Malmsten, *Langmuir*, 2006, **22**, 5476–5484.

6 F. Lim and A. Sun, *Science*, 1980, **210**, 908–910.

7 O. Gåserød, A. Sannes and G. Skjåk-Bræk, *Biomaterials*, 1999, **20**, 773 – 783.

8 H. Sakaguchi, T. Serizawa and M. Akashi, *Journal of Nanoscience and Nanotechnology*, 2006, **6**, 1124–1127.

9 J. Y. Chung, A. J. Nolte and C. M. Stafford, *Advanced Materials*, 2011, **23**, 349–368.

10 C. Stafford, C. Harrison, K. Beers, A. Karim, E. Amis, M. VanLandingham, H. Kim, W. Volksen, R. Miller and E. Simonyi, *Nature Materials*, 2004, **3**, 545–50.

11 B. T. Stokke, K. I. Draget, O. Smidsrød, Y. Yuguchi, H. Urakawa and K. Kajiwara, *Macromolecules*, 2000, **33**, 1853–1863.

12 R. Marcombe, S. Cai, W. Hong, X. Zhao, Y. Lapusta and Z. Suo, *Soft Matter*, 2010, **6**, 784–793.

13 M. H. Ottøy, K. M. Vårum, B. E. Christensen, M. W. Anthonsen and O. Smidsrød, *Carbohydrate Polymers*, 1996, **31**, 253 – 261.

14 S. Tierney, D. R. Hjelme and B. T. Stokke, *Analytical Chemistry*, 2008, **80**, 5086–5093.

15 W. Hong, X. Zhao, J. Zhou and Z. Suo, *Journal of the Mechanics and Physics of Solids*, 2008, **56**, 1779 – 1793.

16 P. J. Flory, *Principles of Polymer Chemistry*, Cornell University Press, 1953.

17 M. K. Kang and R. Huang, *Journal of Applied Mechanics*, 2010, **77**, 061004.

18 L. R. G. Treolar, *The physics of rubber elasticity*, Clarendon Press, 1975.

19 W. Hong, X. Zhao and Z. Suo, *Journal of the Mechanics and Physics of Solids*, 2010, **58**, 558 – 577.

20 G. Decher and J. B. Schlenoff, *Multilayer Thin Films: Sequential Assembly of Nanocomposite Materials*, Wiley-VCH Verlag Gmbh, Weinheim, 2003.

21 U. P. Schröder and W. Oppermann, in *Physical Properties of Polymeric Gels*, J. Wiley & Sons, Chichester, 1996, pp. 19 – 38.

22 B. Guo, A. Elgsaeter, B. E. Christensen and B. T. Stokke, *Polymer Gels and Networks*, 1998, **6**, 471 – 492.

23 A. E. Ehret and M. Böl, *J. R. Soc. Interface*, 2013, **10**, 20120671.

24 K. Gawel, M. Gao and B. T. Stokke, *European Polymer Journal*, 2012, **48**, 1949 – 1959.

25 M. Gao, K. Gawel and B. T. Stokke, *Journal of Colloid and Interface Science*, 2013, **390**, 282 – 290.

26 G. Maurstad, Y. A. Morch, A. R. Bausch and B. T. Stokke, *Carbohydrate Polymers*, 2008, **71**, 672 – 681.

27 I. M. N. Vold, K. A. Kristiansen and B. E. Christensen, *Biomacromolecules*, 2006, **7**, 2136–2146.

28 C. Picart, *Current Medicinal Chemistry*, 2008, **15**, 685–697.

29 M. Tricot, *Macromolecules*, 1984, **17**, 1698–1704.

30 C. G. Baumann, S. B. Smith, V. A. Bloomfield and C. Bustamante, *Proceedings of the National Academy of Sciences*, 1997, **94**, 6185–6190.

31 E. Buhler and F. Boué, *Macromolecules*, 2004, **37**, 1600–1610.

32 H. K. Murnen, A. M. Rosales, A. V. Dobrynin, R. N. Zuckermann and R. A. Segalman, *Soft Matter*, 2013, **9**, 90–98.

33 W. Hong, Z. Liu and Z. Suo, *International Journal of Solids and Structures*, 2009, **46**, 3282 – 3289.

34 S. Tierney, M. Sletmoen, G. Skjåk-Bræk and B. T. Stokke, *Carbohydrate Polymers*, 2010, **80**, 828 – 832.

35 M. Quesada-Perez, J. A. Maroto-Centeno, J. Forcada and R. Hidalgo-Alvarez, *Soft Matter*, 2011, **7**, 10536–10547.

36 T. Hoare and R. Pelton, *Current Opinion in Colloid & Interface Science*, 2008, **13**, 413 – 428.

37 T. Hoare and R. Pelton, *The Journal of Physical Chemistry B*, 2007, **111**, 11895–11906.

38 T. Tanaka, S.-T. Sun, Y. Hirokawa, S. Katayama, J. Kucera, Y. Hirose and T. Amiya, *Nature*, 1987, **325**, 796 – 798.

39 E. Sultan and A. Boudaoud, *Journal of Applied Mechanics*, 2008, **75**, 051002.

40 B. Li, Y.-P. Cao, X.-Q. Feng and H. Gao, *Soft Matter*, 2012, **8**, 5728–5745.

41 G. Ladam, P. Schaad, J. C. Voegel, P. Schaaf, G. Decher and F. Cuisinier, *Langmuir*, 2000, **16**, 1249–1255.